Gender-specific data-driven adiposity subtypes using deep-learning-based abdominal CT segmentation

Article *in* Obesity · May 2023

DOI: 10.1002/oby.23741

14 authors, including:

Xiantong Zou
Peking University People's Hospital
28 PUBLICATIONS **408** CITATIONS
SEE PROFILE

Yufeng Li
Beijing University of Technology
59 PUBLICATIONS **840** CITATIONS
SEE PROFILE

Guotong Xie
PingAn Group
233 PUBLICATIONS **2,032** CITATIONS
SEE PROFILE

Linong Ji
Peking University People's Hospital
607 PUBLICATIONS **16,667** CITATIONS
SEE PROFILE

Received: 22 September 2022 | Revised: 11 January 2023 | Accepted: 11 January 2023

DOI: 10.1002/oby.23741

ORIGINAL ARTICLE

Obesity Biology and Integrated Physiology

Gender-specific data-driven adiposity subtypes using deep-learning-based abdominal CT segmentation

Xiantong Zou[1] | Xianghai Zhou[1] | Yufeng Li[2] | Qi Huang[1] | Yuan Ni[3] | Ruiming Zhang[3] | Fang Zhang[1] | Xin Wen[1] | Jiayu Cheng[1] | Yanping Yuan[1] | Yue Yu[1] | Chengcheng Guo[1] | Guotong Xie[3] | Linong Ji[1]

[1]Department of Endocrinology and Metabolism, Peking University People's Hospital, Beijing, China

[2]Department of Endocrinology, Beijing Friendship Hospital Pinggu Campus, Capital Medical University, Beijing, China

[3]Ping An Technology (Shenzhen) Co., Ltd., Shanghai, China

Correspondence
Linong Ji, Department of Endocrinology and Metabolism, Peking University People's Hospital, Beijing, China.
Email: jiln@bjmu.edu.cn

Guotong Xie, Ping An Technology (Shenzhen) Co., Ltd., Shanghai, China.
Email: xieguotong@pingan.com.cn

Funding information
Beijing Nova Program, Grant/Award Numbers: Z191100001119026, Z211100002121169; National Natural Science Foundation of China, Grant/Award Numbers: 81800515, 81970708

Abstract

Objective: The aim of this study was to quantify abdominal adiposity and generate data-driven adiposity subtypes with different diabetes risks.

Methods: A total of 3817 participants from the Pinggu Metabolic Disease Study were recruited. A deep-learning-based recognition model on abdominal computed tomography (CT) images (A-CT model) was developed and validated in 100 randomly selected cases. The volumes and proportions of subcutaneous fat, visceral fat, liver fat, and muscle fat were automatically recognized in all cases. K-means clustering was used to identify subgroups using the proportions of the four fat components.

Results: The Dice indices among the measurements assessed by the A-CT model and manual evaluation to detect liver fat, muscle fat, and subcutaneous fat areas were 0.96, 0.95, and 0.92, respectively. Three subtypes were generated separately in men and women: visceral fat dominant type (VFD); subcutaneous fat dominant type (SFD); and intermuscular fat dominant type (MFD). Compared with the SFD group, the MFD group had similar diabetes risk, and the VFD group had a 60% higher diabetes risk when age and BMI were adjusted for in men. The adjusted odds ratio for diabetes was 1.92 (95% CI: 1.32-2.78) in the MFD group and 6.14 (95% CI: 4.18-9.03) in the VFD group in women.

Conclusions: This study identified gender-specific abdominal adiposity subgroups, which may help clinicians to distinguish diabetes risk quickly and automatically.

INTRODUCTION

Overweight and obesity have affected almost one-third of the world's population, causing an intensive burden on the global health system due to their associations with many metabolic disorders, including diabetes, hypertension, dyslipidemia, and cardiovascular disease [1]. In addition to excess adiposity, the distribution of adipose tissue also contributes to the development of metabolic disorders and cardiovascular diseases [2]. Visceral adipose tissue (VAT) has been suggested to be more hazardous than subcutaneous adipose tissue (SAT) because the former has a stronger independent association with cardiovascular risk factors than the latter [3, 4]. Ectopic fat deposition, e.g., in the liver and skeletal muscle, is highly associated with increased VAT [5, 6]. The role of hepatic fat accumulation and VAT deposition is of high interest for early recognition and timely intervention to prevent metabolic disease, and their associations with cardiometabolic disorders have been described in many studies [7–10]. There is still clinical demand to identify diabetes risk of different fat distribution patterns in a quick and automatic manner.

Xiantong Zou, Xianghai Zhou, and Yufeng Li had equal contribution to this work.

Magnetic resonance imaging (MRI), computed tomography (CT), dual-energy x-ray absorptiometry scans, and body composition analyzers are commonly accepted methods to assess the abdominal fat distribution. Abdominal CT is a powerful tool to identify abdominal organs and quantify abdominal adiposity, and semiautomatic tools have been routinely used in studies to measure fat areas on selected layers or multiple layers [11, 12]. Data-driven subgroups derived according to manually measured fat distribution parameters on abdominal CT scans have shown distinct diabetes risks [13]. Nevertheless, the manual measurement may require experience and excess time, which may impede the clinical application of these subgroups. Advances in deep-learning-based image recognition techniques have enabled quick quantification of abdominal adiposity [14]. In addition, automatic quantification of hepatic steatosis has been developed and applied in population-based studies [15]. Image recognition of whole-body MRI scans has also provided high diagnostic accuracy toward diabetes prediction [16]. In this study, we aimed to apply automatic image recognition on CT to quantify the volumes of abdominal adiposity, including SAT, VAT, liver fat, and skeletal muscle fat, and to generate novel adiposity subtypes in a large cross-sectional epidemiological study.

Study Importance

What is already known?

- Different types of distribution of abdominal adiposity convey different diabetes risks.
- A method to quickly detect different adiposity distributions was missing.

What does this study add?

- Deep-learning-based computed tomography (CT) segmentation identified visceral fat, subcutaneous fat, liver fat, and muscle fat and calculated their proportions in a large Chinese cross-sectional cohort.
- Gender-specific subgroups with distinct diabetes risks were identified using these new measurements.

How might these results change the direction of research or the focus of clinical practice?

- The diabetes risk of a patient having an abdominal CT test can be quickly and automatically detected with this tool.

METHODS

The flowchart of the study design is presented in Figure 1.

Study population

The Pinggu Metabolic Disease Study was a sequential epidemiological survey conducted from 2012 to 2014, as previously described [17]. Briefly, citizens from neighborhood communities in the Pinggu District of Beijing, China, were randomly drawn and invited using a two-stage cluster random sampling method. Five rural towns and one street were randomly selected at the first stage, and then five villages and seven neighborhood communities were randomly drawn from each selected rural town and street. From September 2013 to July 2014, a total of 6583 residents were invited, and 4002 individuals aged 26 to 76 years were enrolled (response rate 60.8%).

We excluded 32 participants without CT scans, 22 participants without key variables, 5 participants in whom it was difficult to decide the presence of diabetes, and 126 participants in whom we were unable to apply automatic image recognition. Finally, 3817 participants were included in the final analysis (Supporting Information Figure S1).

The Pinggu Metabolic Disease Study was approved by the ethics committees of Peking University Medical Centre and the University of Michigan. All participants gave written informed consent.

Clinical measurements

Questionnaires on the characteristics of participants were collected by trained doctors and nurses in the local clinics. Body mass index (BMI) was calculated as weight in kilograms divided by height in meters squared. Waist circumference (WC) was measured at the middle point level between the lower rib margin and the iliac crest. Blood pressure was measured three times at 10-minute intervals, and the average was used. Current smoking was defined as participants with average daily consumption of more than one cigarette. Excess alcohol consumption (grams per week) was defined as pure alcohol > 210 g/wk in men and >140 g/wk in women.

Fasting blood samples were collected for biochemical tests in the central lab in Peking University People's Hospital in Beijing. Participants without known diabetes underwent a 75-g 2-hour oral glucose tolerance test, and those with known diabetes had only fasting plasma glucose measured. Plasma glucose levels were measured using a hexokinase method. Serum total cholesterol, triglycerides, high-density lipoprotein cholesterol, low-density lipoprotein cholesterol, alanine aminotransferase, aspartate aminotransferase, and creatine were measured using an automated clinical chemistry analyzer (UnicelDxC 800; Beckman Coulter Inc., Brea, California). Hemoglobin A_{1c} was measured using cation-exchange high-pressure liquid chromatography (Adams A1c HA-8160; ARKRAY, Kyoto, Japan), and insulin levels were measured using electrochemiluminescence immunoassay, as previously described [17, 18]. Homeostasis model assessment to measure insulin resistance (HOMA-IR) and β-cell function (HOMA-B) were measured using the following equations:

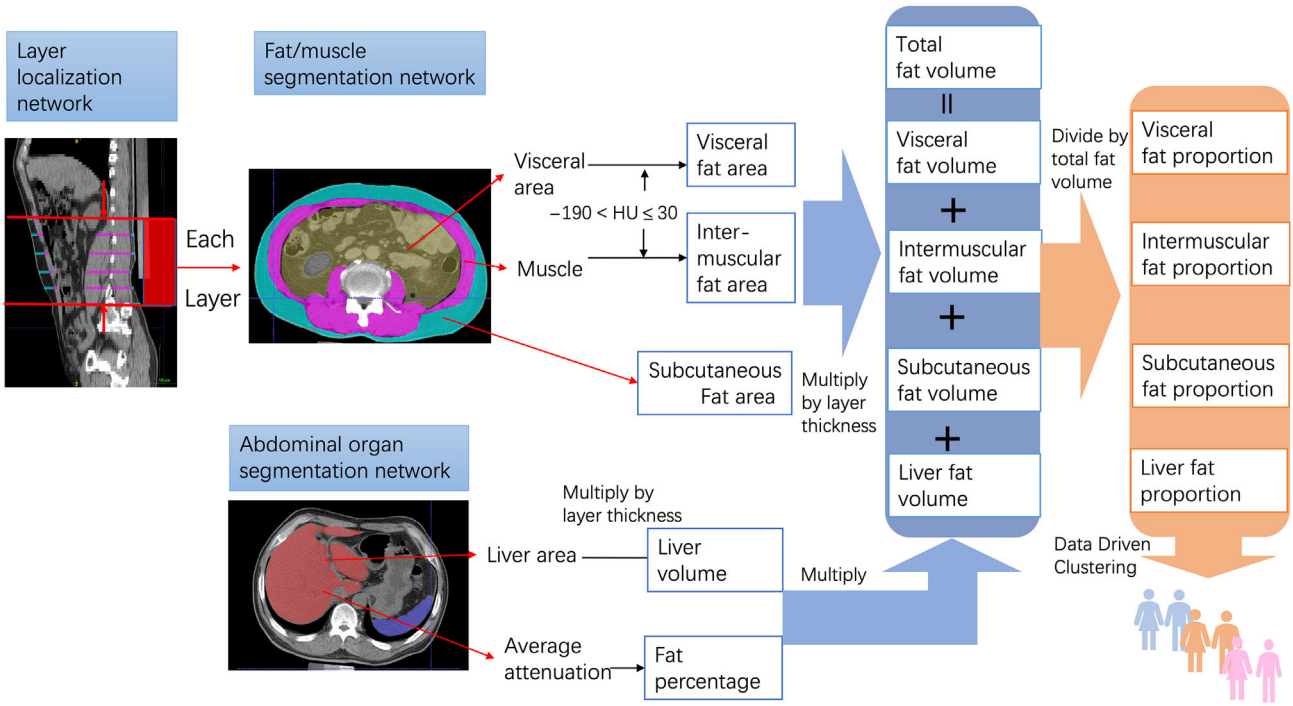

FIGURE 1 Flowchart of the study procedure. Briefly, two deep-learning-based algorithms (A-CT model) were applied. The abdominal muscle area and subcutaneous fat area were automatically recognized by the A-CT model. On each layer between T12-L1 and L5-S1, the visceral fat area and intermuscular fat area were calculated as the areas with HU between −190 and 30 within the inner line of the abdominal cavity and within the muscle area. The liver area in each visible layer was recognized, and liver volume was obtained by adding all liver areas multiplied by layer thickness. The average attenuation of all liver areas was calculated and converted to the total liver fat percentage. Liver fat volume was calculated by multiplying liver volume and liver fat percentage. Total abdominal fat volume was calculated by adding the four compartments' fat volumes. The proportions of the four fat compartments were calculated by dividing the volume of each compartment by total fat volume. Four proportion parameters were used to conduct data-driven clustering in male and female individuals, separately. A-CT, abdominal computed tomography; HU, Hounsfield unit [Color figure can be viewed at wileyonlinelibrary.com]

$$\text{HOMA}-\text{IR} = (\text{Fasting insulin}\,[\mu\text{IU/mL}]) \times (\text{Fasting plasma glucose}\,[\text{mmol/L}])/22.5$$

$$\text{HOMA}-\text{B} = 20 \times (\text{Fasting insulin}\,[\mu\text{IU/mL}]) / (\text{Fasting plasma glucose}\,[\text{mmol/L}]) - 3.5)$$

Definition of disease and conditions

Diabetes was defined according to World Health Organization 1999 criteria: 1) previously reported history of diabetes or on glucose-lowering therapy; and 2) fasting glucose ≥ 7.0 mmol/L or postprandial glucose during oral glucose tolerance test ≥11.1 mmol/L. Obesity was defined as BMI ≥ 28 kg/m^2, and central obesity was defined as WC ≥ 90 cm in men and WC ≥ 85 cm in women, according to the guideline of obesity management in China [19].

Measurements of abdominal adiposity using CT

Individuals underwent an unenhanced abdominal CT scan in the supine position using a 64-slice multidetector scanner (LightSpeed VCT; General Electric Healthcare, Milwaukee, Wisconsin) with 5-mm-thick interval under 120 kV (peak), 120 to 150 mA from the lung base to the pubic symphysis.

Manual evaluation

Liver fat was measured using the region of interest (ROI) method by an experienced physician (Fang Zhang). The Hounsfield units (HU) of three randomly selected 1-cm^2 areas of liver and spleen, avoiding the vessels, were acquired and averaged. Fatty liver was defined as liver/spleen HU ≤ 1.1, as previously described [17]. Visceral fat area (VFA) and subcutaneous fat area (SFA) were derived by analysis of the CT image at L4-5 vertebrate interval using ImageJ version 1.34e software packages (National Institutes of Health, Bethesda, Maryland) by an experienced physician. The cross-sectional areas (millimeters squared) of total fat area were calculated using standard HU ranges (−190 to −30 for adipose tissue), as recommended by previous research [20]. VFA was quantified as fat areas inside the inner line of the muscle wall surrounding the abdominal cavity, and SFA was defined as total fat area − VFA, as previously described [21].

Artificial intelligence-facilitated measurements: validation and application of the A-CT model

Abdominal adipose tissue and muscle

The automatic image recognition model was a novel two-step method that was developed and validated in a Chinese cohort with 293 participants [22]. The model automatically localizes the vertebrate interval and recognizes the muscle, SAT, and VAT based on a segmentation network, and a cross-stage attention block and an adversarial structure are jointly used in tissue segmentation to enhance the performance (Supporting Information Figure S2). The model achieved 95% Dice for localization and segmentation.

In our study, the model was further trained and validated using human-labeled CT scans in the experimental cohort. The CT scans of 100 randomly selected participants were labeled back to back by two experienced physicians (Jiayu Cheng and Yanping Yuan, both with more than 3 years of clinical work experience) who were trained by an experienced radiologist with more than 3 years of work experience. The labels of Person 1 were used for model validation, and the labels of Person 2 were used for comparison. The labels included six layers of CT images on the vertebrate intervals from T12-L1 to L5-S1. SFA was labeled as the area between the outline of the muscle wall and the abdominal surface. The muscle area included all muscles in the abdominal cavity (including psoas, paraspinal, and abdominal wall musculature), as previously described [23]. The deviation cohort contained 80 randomly selected cases, and the internal validation cohort contained 20 randomly selected cases. The accuracy of this A-CT model was assessed in the internal validation cohort.

The A-CT model localizes T12-L1 and L5-S1 and then recognizes all layers with 5-mm intervals among these two layers. SFA was automatically recognized by the A-CT model. Areas within the HU range of −30 to −190 inside the recognized muscle area were defined as the intermuscular fat area. Intermuscular fat percentage was calculated as the average ratio of the muscle fat area to the muscle area. VFA was the area with the HU range of −30 to −190 within the inner line of the muscle, which was automatically picked up by the A-CT model when the inner line of the abdominal cavity was localized. Areas were selected as pixels, converted to centimeters squared, and then multiplied by the thickness of the layers to obtain the fat and organ volumes (centimeters cubed). The VAT, SAT, and muscle volumes were confined to T12-L1 and T5-S1, as previously described [24].

Liver fat volume

The liver was labeled back to back on each visible layer by two experienced physicians (Jiayu Cheng and Yanping Yuan as Person 1 and Person 2, similar to the abdominal fat and muscle labels). A deep-learning algorithm was used to segment the liver by learning the labels of Person 1 in the deviation cohort (Supporting Information Figure S3), and model accuracy was assessed in the internal validation cohort as the abdominal fat segmentation network. The total volume of the liver and the average CT value of the liver were acquired by the A-CT model. The liver fat percentage was calculated using the following equation [15]:

$$\text{CT fat percentage} = (\text{CT HU}) \times (-0.58) + 38.2.$$

The total volume of the liver fat was calculated by multiplying the fat percentage and the liver volume.

Detailed methods for deep learning are presented in Supporting Information Figures S2 and S3.

Data-driven cluster analysis

The proportions of liver fat, subcutaneous fat, visceral fat, and intermuscular fat were calculated as the volume of each fat compartment divided by total fat volume (the sum of four fat components). Fat proportions of each compartment were standardized, and data-driven clustering was performed separately in male and female individuals. K-means clustering was used to allocate the participants into subgroups, and the optimal *K* value was determined using average silhouette width by R (version 3.6.3; Vienna, Austria). We ran the clustering with 25 initial configurations and selected the most stable cluster for further analysis. Finally, three clusters were generated, namely the subcutaneous fat deposition subtype (SFD), visceral fat deposition subtype (VFD), and muscle fat deposition subtype (MFD).

Sensitivity analysis was conducted using different parameters related to abdominal fat to generate data-driven subtypes. The clinical characteristics of clusters were analyzed, and clusters were selected according to their clinical significance.

Statistical analysis

All of the deep-learning models are implemented under the Keras/Tensorflow framework. The train/test experiments are operated on Nvidia V100 graphics processing units (GPUs) (16 GB). The average processing time (with preprocess + three segmentation models + postprocess) for a single case is approximately 2 minutes. Dice similarity coefficients and Bland–Altman comparison figures were used to assess the accuracy of the A-CT model in the internal validation cohort.

Statistical analysis was conducted in Stata version 16.0 (StataCorp LLC, College Station, Texas) and R (version 3.6.3). Continuous variables with normal distribution were presented as mean (standard deviation [SD]) and compared using *t* test. Variables with skewness were presented as median (interquartile range) and compared using Mann–Whitney *U* tests. Categorical data were presented as number and percentage and compared using χ^2 tests.

Lasso regression with fivefold cross validation was used to assess the coefficients of adiposity measurements and diabetes. Logistic

regression in crude or adjusted for age, gender, and BMI was used to assess the associations among diabetes and adiposity measurements. The clinical characteristics of the data-driven adiposity clusters were assessed. Finally, we assessed the association of diabetes in models in crude or adjusted for age, gender, and BMI or WC if appropriate.

A significant difference was defined as two-sided $p < 0.05$.

RESULTS

Validation of deep-learning-based CT segmentation (A-CT model)

We randomly selected 100 participants from all participants to develop and validate our model for CT segmentation. The 100 cases were randomly divided into a deviation cohort (80 samples) and an internal validation cohort (20 samples). The Dice coefficient of liver segmentation was 0.96 between the A-CT model and Person 1 and 0.98 between Person 1 and Person 2. The Dice coefficient for SFA and muscle area was 0.95 and 0.92 between Person 1 and the A-CT model and 0.93 and 0.88 between Person 1 and Person 2 at layer T12-L1 and L5-S1, respectively. The accuracy of the A-CT model to detect VFA was mainly dependent on the accuracy to detect muscle area according to the method we used. The Bland–Altman comparison figures are presented in Figure 2A-2C.

We then applied the A-CT model to all of the 3817 participants we recruited. The abdominal SAT volume and VAT volume were highly correlated to the corresponding fat area at layer L4-5 measured by a human individual (Pearson R for SAT and VAT was 0.936 and 0.913, respectively, with both $p < 0.001$; Figure 2D-2E). The distribution of liver attenuation quantified by the A-CT model was similar to the liver CT attenuation quantified manually (Figure 2F-2G). The liver fat volume calculated by the A-CT model was significantly correlated to the liver-spleen ratio measured by the manual ROI method (Pearson $R = 0.604$, $p < 0.001$; Figure 2H).

The association between abdominal fat distribution and diabetes

The prevalence of diabetes was 18.75% among all participants. Compared with participants without diabetes, participants with diabetes had higher BMI and subcutaneous, visceral, liver, and muscle fat volumes. The proportions of visceral fat and liver fat were higher and the subcutaneous fat and muscle fat proportions were lower in participants with diabetes (Supporting Information Table S1).

All abdominal fat volumes were positively associated with diabetes in crude; however, after adjusting for age, sex, and BMI, subcutaneous fat volume and muscle fat percentage were nonsignificantly related to diabetes, and muscle fat volume was negatively associated with diabetes. The adjusted odds ratio (OR) and 95% confidence interval (CI) for diabetes was 1.828 (95% CI: 1601-2.087) and 2.091 (95% CI: 1.896-2.326) per SD increase in visceral fat volume and liver fat volume, respectively. To avoid multicollinearity, we used Lasso regression correcting for age, BMI, and sex to investigate the associations among diabetes and four fat components together, which suggested the coefficients for per-SD increase in liver fat volume and visceral fat volume ranked in first and second place (Table 1).

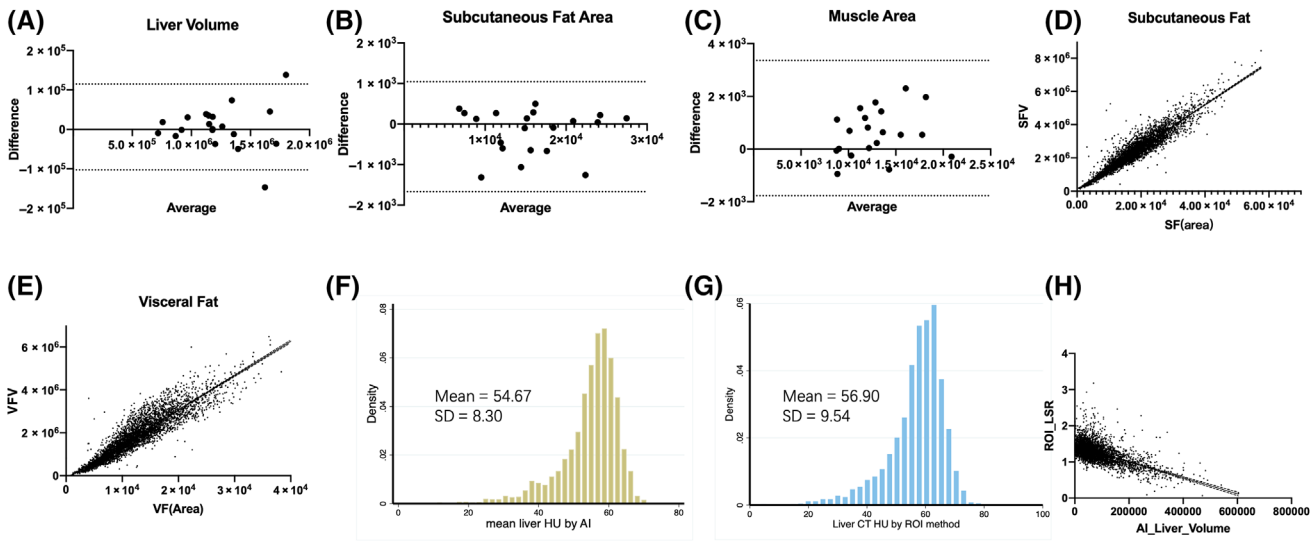

FIGURE 2 Validation of the A-CT model. Bland–Altman comparison figure between the A-CT model and a human individual (Person 1) in the validation cohort in (A) liver volume, (B) subcutaneous fat area, and (C) muscle area, both at layer T12-L1 and L5-S1. (D,E) Correlation between fat area (millimeters squared) measured manually by a human individual or fat volume (millimeters cubed) recognized by the A-CT model. (F,G) Histograms showing the distribution of the average liver CT attenuation measured by the (F) A-CT model and (G) ROI. (H) Correlation between the liver-spleen ratio (LSR) measured by a human individual manually and liver fat volume (millimeters cubed) recognized by the A-CT model. A-CT, abdominal computed tomography; AI, artificial intelligence; HU, Hounsfield unit; ROI, region of interest [Color figure can be viewed at wileyonlinelibrary.com]

TABLE 1 Logistic regression and Lasso logit regression between diabetes and abdominal adiposity and fat distribution

	Logistic regression		Lasso coefficient (adjusted for age, sex, and BMI)
	Unadjusted	Adjusted (for age, gender, and BMI)	
Subcutaneous fat volume	1.201 (1.111-1.299)*	0.921 (0.775-1.094)	0
Visceral fat volume	1.935 (1.781-2.102)*	1.828 (1601-2.087)*	0.499
Liver fat volume	1.854 (1.719-2.001)*	2.091 (1.896-2.326)*	1.145
Intermuscular fat volume	1.035 (1.027-1.043)*	0.978 (0.841-1.000)*	−0.178
Intermuscular fat percentage	1.319 (1.216-1.433)*	0.897 (0.797-1.009)	/
Liver fat percentage	1.956 (1.808-2.116)*	1.968(1.787-2.165)*	/
Subcutaneous fat proportion	0.503 (0.458-0.551)*	0.464 (0.401-0.530)*	0
Visceral fat proportion	1.900 (1.739-2.077)*	1.900 (1.668-2.163)*	0.5501
Liver fat proportion	1.746 (1.604-1.900)*	1.889 (1.713-2.082)*	0.682
Intermuscular fat proportion	0.882 (0.810-0.960)*	0.685(0.611-0.768)*	−0.235

Note: The odds ratio (95% CI) for diabetes of each abdominal adiposity index was calculated individually in an unadjusted logistic regression model and logistic regression models adjusted for age, gender, and BMI. The first Lasso logit model contained four fat volumes, the second Lasso model included fat proportions, and both models were adjusted for age, gender, and BMI. For liver and muscle adiposity indices that were not normally distributed, data were log-transformed. All data were standardized using mean and SD in men and women separately.
Abbreviation: DM, diabetes mellitus.
*$p < 0.001$.

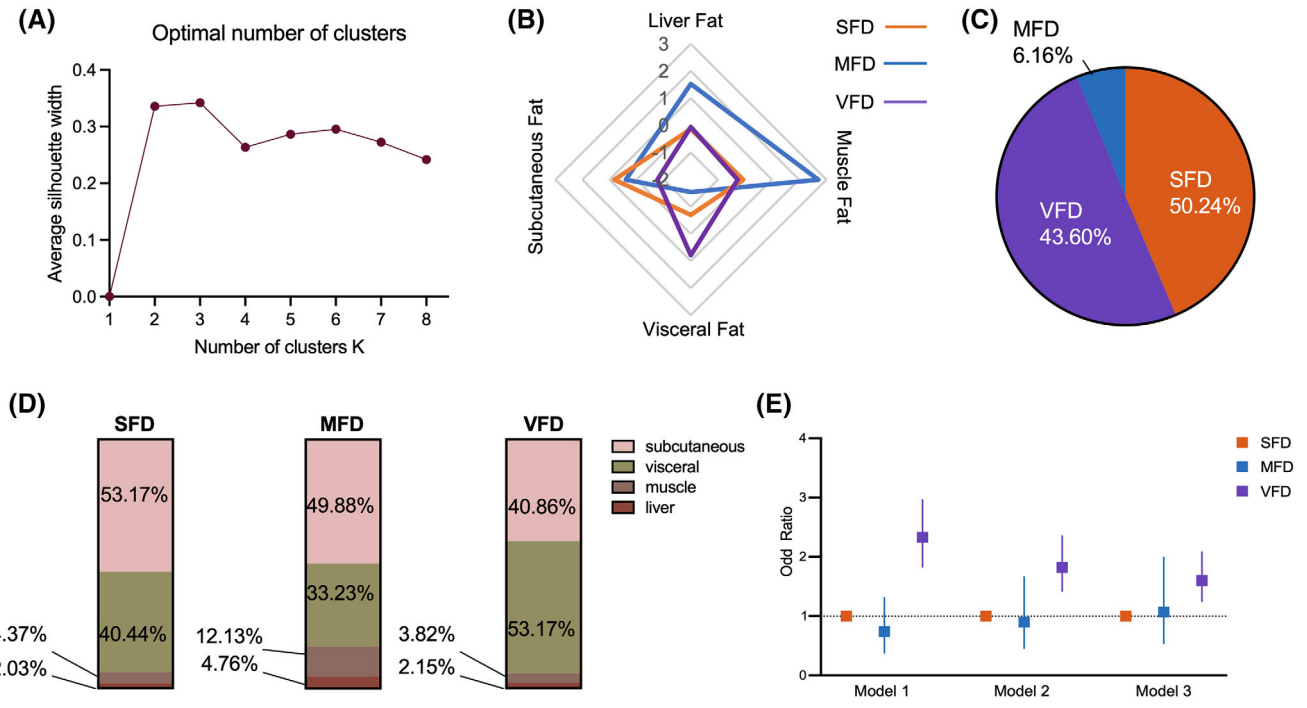

FIGURE 3 Characteristics of data-driven subtypes in male individuals. (A) Identifying the optimal *K* value for cluster analysis using the average silhouette width. (B) Spider chart of three subtypes describing the proportions of visceral fat, subcutaneous fat, muscle fat, and liver fat. Data were scaled as per SD difference. (C) Ratio of each subtype within the total population. (D) Composition of fat proportions in the three subtypes. The median of the proportions of four fat compartments is presented. (E) Odds ratio (95% CI) for diabetes of each subtype in reference to SFD in models unadjusted (model 1), adjusted for age and BMI (model 2), and adjusted for age and waist circumference (model 3). MFD, muscle fat dominant subtype; SFD, subcutaneous fat dominant subtype; VFD, visceral fat dominant subtype [Color figure can be viewed at wileyonlinelibrary.com]

The distribution of the volumes and proportions of the four fat compartments is presented in Supporting Information Figure S4. The subcutaneous and muscle fat proportions were negatively associated with diabetes in crude and after adjustment. Per-SD increases in the proportions of liver fat and visceral fat were both associated with a 90% increase in diabetes risk after age, BMI, and sex were adjusted

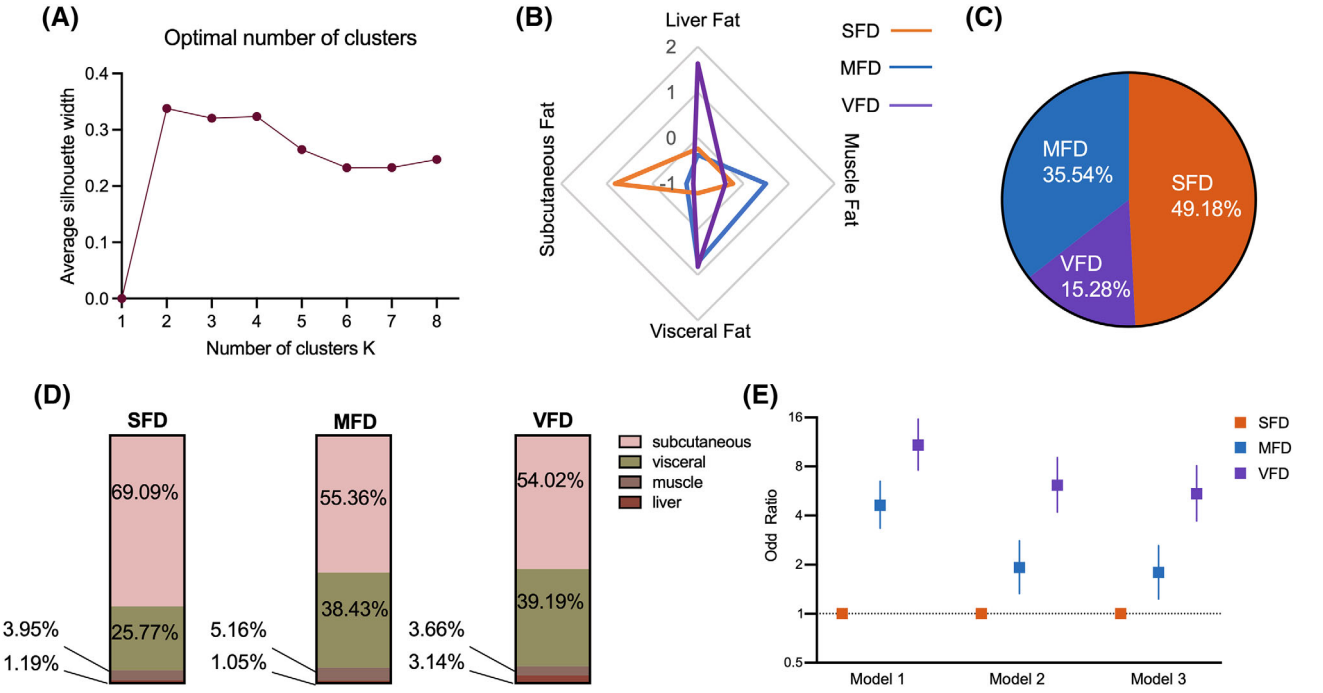

FIGURE 4 Characteristics of data-driven subtypes in female individuals. (A) Identifying the optimal *K* value for cluster analysis using the average silhouette width. (B) Spider chart of three subtypes describing the proportions of visceral fat, subcutaneous fat, muscle fat, and liver fat. Data were scaled as per SD difference. (C) Ratio of each subtype within the total population. (D) Composition of fat proportions in the three subtypes. The median of the proportions of four fat compartments is presented. (E) Odds ratio (95% CI) for diabetes of each subtype in reference to SFD in models unadjusted (model 1), adjusted for age and BMI (model 2), and adjusted for age and waist circumference (model 3). MFD, muscle fat dominant subtype; SFD, subcutaneous fat dominant subtype; VFD, visceral fat dominant subtype [Color figure can be viewed at wileyonlinelibrary.com]

for. The coefficients of Lasso logit for diabetes were 0, 0.550, 0.682 and −0.235 for per-SD increases in proportions of subcutaneous fat, visceral fat, liver fat, and muscle fat after adjustment (Table 1).

Gender-specific data-driven abdominal fat deposition subtypes and their association with diabetes

Because the fat distribution patterns were different between male and female individuals, we performed k-means clustering in men and women separately. In men, the optimal *K* value was determined as 3 (Figure 3A). Three subtypes were generated and named as SFD, VFD, and MFD according to the clinical characteristics. The SFD was the dominant subtype (50.24% of all male individuals), with the highest proportion of subcutaneous fat (53.17% of total fat volume). A total of 43.6% of participants were in the VFD group, and they had the highest visceral fat proportion (53.17% of total fat volume). The MFD group, which had only around 6% of male individuals, had the highest intermuscular fat proportion (12.13%) and hepatic fat proportion (4.76%; Figure 3B-3D). The MFD group showed similar diabetes risk with the SFD group, with or without adjustment for confounders. Being a member of the VFD group was independently significantly associated with a 60% to 80% higher diabetes risk compared with the SFD group, even after age and BMI/WC were adjusted for (OR for diabetes was 0.90 [95% CI: 0.47-1.71] in the MFD group and 1.82 [95% CI: 1.42-2.34] in the VFD group after adjusting for age and BMI; and 1.07 [95% CI: 0.56-2.05] in the MFD group and 1.60 [95% CI: 1.24-2.07] after adjusting for age and WC; Figure 3E).

In women, the optimal *K* value could be 2 to 4, and we selected 3 as the cluster number to keep consistent with the clusters in the male individuals (Figure 4A). SFD was also the dominant subtype (49.18% of all female individuals) with the highest subcutaneous fat proportion (69.09%). MFD was the second largest group (35.54% of all female individuals), which was characterized by the highest level of intermuscular fat proportion. The VFD group had only 15.28% of female individuals, with the highest visceral fat proportion (54.02%) and liver fat proportion (3.14%; Figure 4B-4D). Being a member of both the MFD and VFD groups was associated with a higher diabetes risk related to SFD in crude. After adjustment for age and BMI, the OR for diabetes was 1.92 (95% CI: 1.32-2.78) in the MFD group and 6.14 (95% CI: 4.18-9.03) in the VFD group; the adjusted OR for diabetes was 1.78 (95% CI: 1.23-2.60) in the MFD group and 5.44 (95% CI: 3.69-8.03) in the VFD group when age and WC was controlled. The characteristics of both men and women are presented in Supporting Information Table S2. In men, the VFD group had the highest BMI and WC, and the MFD group had the oldest age and lowest BMI and WC. In women, the MFD group had the oldest age, and the VFD

group had the highest BMI and WC (Supporting Information Table S2).

In the sensitivity analysis, we generated three clusters in all participants rather than clustering separately in female and male individuals, and the characteristics mainly recapitulated the male cluster (Supporting Information Figure S5). We also tried to replace the parameters using average muscle HU, average liver HU, liver fat percentage, or total muscle fat percentage. However, in these analyses, the optimal cluster number was 2, which was SFD and VFD (Supporting Information Figures S6-S9).

DISCUSSION

In this study, we used autonomous CT image recognition to acquire abdominal fat volumes rather than relying on manual measurement. The semiautomatic assessment of visceral fat and subcutaneous fat using axial CT images has been widely used in studies [11]. In the past decade, abdominal CT segmentation, mainly based on a U-shaped network, has rapidly developed and has reached >90% accuracy in most organs [25–27]. Artificial intelligence for CT image recognition has been widely used to assist doctors in improving diagnosis efficiency as a medical assistant platform [28], rather than as a replacement for human work, because of the high requirement of clinical safety and the heterogeneity among individuals. Validation and repeatability were key considerations for artificial intelligence machines in clinical studies. We have taken a few steps to validate the A-CT model in our study. The A-CT model was developed previously [22] and further validated in randomly selected samples in our study. For SAT and muscle, the A-CT model reached even higher Dice indices than Person 2. We compared the liver HU value measured by the A-CT model and by human individuals using ROI in all 3817 cases, and the results were highly consistent. We also compared the visceral and subcutaneous fat volumes with fat areas at the L4-5 layer quantified by human individuals in all 3817 participants, and the fat volumes were highly associated with manual measurements. By applying the A-CT model, we were able to expand the research sample size, save human work, and develop novel adiposity measurements.

Many radiological methods such as dual-energy x-ray absorptiometry, MRI, and CT have been used to measure abdominal adiposity. Only CT and MRI meet our needs because they provide direct detection of subcutaneous and visceral fat [12, 29]. In current practice, MRI proton density fat fraction has been accepted as the noninvasive gold standard for fatty liver in clinical trials [30]. There has been a good correlation among nonenhanced CT and proton density fat fraction or histology in measuring hepatic fat content [31, 32]. Moreover, automatic hepatic segmentation and fat quantification have been validated in a population-based cohort as a screening tool for fatty liver [15]. Accordingly, unenhanced abdominal CT can provide quick acquisition, high resolution, and accurate fat measurement for our purpose.

Different patterns of abdominal fat distribution harbor different metabolic risks. Many studies have suggested that VAT predicted more metabolic and cardiovascular risk than SAT [33, 34], and the distribution of the abdominal fat in the liver or in the visceral bed has been frequently investigated [7, 8, 35]. We quantified the fat volumes of VAT, SAT, liver fat, and intermuscular fat together and generated novel adiposity measurements, which were the proportions of fat in each compartment to better describe the fat distribution. The distribution patterns of the four proportion parameters were slightly different than the fat volumes of each compartment (Supporting Information Figure S4). Abdominal fat mainly deposits in the subcutaneous and visceral beds, and ectopic fat makes up less than 10% of total abdominal fat. Nevertheless, the parameters were standardized in both genders; therefore, the cluster characteristics were mainly affected by the relative difference within the group in each parameter rather than the difference among the parameters in a specific person. In the sensitivity analysis, we tried a few combinations of parameters to form the data-driven clusters; however, the clusters may not deliver more information other than the SFD or VFD phenotype (Supporting Information Figures S5-S9). Additionally, the distribution patterns of fat in both genders were different. Women were characterized by more subcutaneous fat and less visceral fat, and men had the opposite phenotype. By this means, we generated gender-specific clusters using the four novel parameters.

In both male and female individuals, VFD carried the highest diabetes risk compared with SFD because VFD had the highest visceral fat proportions. MFD carried intermediate risk for diabetes among the three groups in women and similar risk for diabetes with SFD in men. In fact, MFD in men and MFD in women were not similar, although they all had the highest intermuscular fat proportions. In men, MFD included a small group of lean, elderly individuals with the highest muscle fat and hepatic fat proportions but the lowest visceral fat proportion. There is evidence that intermuscular fat accumulation may trigger muscle insulin resistance and local inflammation, thus increasing diabetes risk [36]; therefore, it has been positively associated with diabetes risk [37]. The extent of myosteatosis in MFD may be different between genders because the average intermuscular fat proportions were 12% in men and 5% in women. In this specific subgroup of men, the effect of muscle fat accumulation and hepatic fat accumulation may be overridden by other characteristics, including lower BMI and WC values. They were possibly a group of individuals who were older, who were lean, and who had nonalcoholic fatty liver disease, with the lowest visceral fat proportions. In women, VFD had the highest hepatic fat proportion, and this may explain why this group conveyed the highest diabetes risk among the three groups, although the visceral fat proportions were almost identical between VFD and MFD.

The clinical utility of our study is to facilitate metabolic risk stratification during CT scans. Different from other cluster studies [38], our adiposity subtypes were independent of any metabolic biomarkers or anthropometric measurements. Another study has generated subgroups using fat compartments, including the liver, VFA, and pancreas, and found that subgroups with fat deposition in the liver, pancreas, and visceral fat all carried a higher diabetes risk than the subgroup

with steatopenia (low levels of fat) [13]. However, our model used an automatic recognition model rather than a manual measurement [13]. A supervised deep-learning-based algorithm derived using abdominal MRI also has been applied to predict the precise diabetes risk [16]. Our A-CT recognition and data-driven subgroup module can be easily installed on CT machines to generate adiposity subtypes, providing clinicians with quick information about diabetes risk without clinical examination and biochemical tests.

According to our knowledge, our study is the first study to assess liver, muscle, VAT, and SAT using deep-learning-based automatic image recognition, and it generated four novel parameters describing fat proportions in one study in a large Chinese population. We identified gender-specific subtypes, which carried different risks for diabetes without other clinical measurements. However, we do have a few limitations: 1) We are unable to quantify the pancreas fat volume, which was suggested to be related to diabetes [39], because of limited recognition accuracy. The Dice index for the pancreas in our system can reach only 0.73 to 0.80, which was far behind the accuracy of other organs. 2) Given the inherent limitations of noncontrast CT, we could not reliably exclude blood vessels, which may lead to lower HU and higher fat percentage in the liver. Also, the measurement for fatty liver by CT was outperformed by dual gradient echo MRI and proton magnetic resonance spectroscopy in the diagnosis of fatty liver [40]. 3) We validated our model in a relatively small sample size. However, our model was previously derived in other cohorts, and other studies that used a similar validation sample size have achieved high accuracy as well [41, 42]. Thus, participants in the Pinggu cohort were homogeneous because all participants were recruited from the same district in Beijing, and all participants were scanned using the same CT machine. 4) Rather than measuring adipose tissue from the diaphragm to the pelvic floor, we measured the abdominal fat volume only from T12-L1 to L5-S1, as previously described [24]. The fat volume was almost half of the previously reported whole-body visceral fat [42]. In addition, our calculations underestimated the actual muscle and hepatic fat volumes. We were unable to calculate the intramuscular fat, the liver fat converted from the equation was originally designed to describe fat-weight percentage, and our calculations may lead to underestimation of liver fat volume as well. However, this should not affect our cluster analysis because all variables were standardized and the characteristics were defined by the relative relationship among individuals. 5) There is a lack of external validation of our cluster analysis; therefore, the external generalizability of the subtypes we derived was yet to be tested. 6) Our study is a cross-sectional study without prognostic data; therefore, there was no causal relationship that can be gained.

CONCLUSION

A deep-learning-based automatic CT image recognition model successfully identified the volumes of liver fat, muscle fat, VAT, and SAT. VAT and hepatic fat volumes or proportions were positively associated with diabetes. Gender-specific data-driven clusters generated using proportions of liver fat, visceral fat, and subcutaneous fat had distinct diabetes risks. With further validation, these adiposity subtypes can be implemented to help clinicians and radiologists to identify individuals who carry higher metabolic risks without other clinical measurements.

AUTHOR CONTRIBUTIONS

Xiantong Zou designed the study, analyzed the data, and wrote the manuscript. Xianghai Zhou contributed to data collection, data analysis, and manuscript writing. Yufeng Li contributed to data collection and analysis. Qi Huang contributed to data collection and data analysis during the revision. Ruiming Zhang and Ni Yuan validated and applied the abdominal computed tomography (A-CT) model. Fang Zhang, Xin Wen, Jiayu Cheng, Yanping Yuan, Yue Yu, and Chengcheng Guo contributed to data collection. Guotong Xie and Linong Ji contributed to study design and revised the manuscript.

FUNDING INFORMATION

This work was supported by Beijing Nova Program of Science and Technology (Z191100001119026) and Beijing Nova Cross program (Z211100002121169; to Xiantong Zou); and the National Natural Science Foundation of China (81970708 to Linong Ji and 81800515 to Xiantong Zou) The funders had no roles in study design and or in the decision to publish the results.

DATA AVAILABILITY STATEMENT

Data are kept by Linong Ji and Guotong Xie and can be retrived under reasonable requests.

CONFLICT OF INTEREST

The authors declared no conflict of interest.

ORCID

Linong Ji https://orcid.org/0000-0002-3262-2168

REFERENCES

1. NCD Risk Factor Collaboration (NCD-RisC). Worldwide trends in body-mass index, underweight, overweight, and obesity from 1975 to 2016: a pooled analysis of 2416 population-based measurement studies in 128·9 million children, adolescents, and adults. *Lancet*. 2017;390(10113):2627-2642.
2. Neeland IJ, Ross R, Després JP, et al. Visceral and ectopic fat, atherosclerosis, and cardiometabolic disease: a position statement. *Lancet Diabetes Endocrinol*. 2019;7(9):715-725.
3. Neeland IJ, Ayers CR, Rohatgi AK, et al. Associations of visceral and abdominal subcutaneous adipose tissue with markers of cardiac and metabolic risk in obese adults. *Obesity (Silver Spring)*. 2013;21(9):E439-E447.
4. Abraham TM, Pedley A, Massaro JM, Hoffmann U, Fox CS. Association between visceral and subcutaneous adipose depots and incident cardiovascular disease risk factors. *Circulation*. 2015;132(17):1639-1647.
5. Samuel VT, Shulman GI. Nonalcoholic fatty liver disease as a nexus of metabolic and hepatic diseases. *Cell Metab*. 2018;27(1):22-41.
6. Kurinami N, Sugiyama S, Morita A, et al. Ratio of muscle mass to fat mass assessed by bioelectrical impedance analysis is significantly correlated with liver fat accumulation in patients with type 2 diabetes mellitus. *Diabetes Res Clin Pract*. 2018;139:122-130.

7. Magkos F, Fabbrini E, Mohammed BS, Patterson BW, Klein S. Increased whole-body adiposity without a concomitant increase in liver fat is not associated with augmented metabolic dysfunction. *Obesity (Silver Spring)*. 2010;18(8):1510-1515.
8. Liu J, Fox CS, Hickson D, Bidulescu A, Carr JJ, Taylor HA. Fatty liver, abdominal visceral fat, and cardiometabolic risk factors: the Jackson Heart Study. *Arterioscler Thromb Vasc Biol*. 2011;31(11):2715-2722.
9. Nobarani S, Alaei-Shahmiri F, Aghili R, et al. Visceral adipose tissue and non-alcoholic fatty liver disease in patients with type 2 diabetes. *Dig Dis Sci*. 2022;67(4):1389-1398.
10. Tejani S, McCoy C, Ayers CR, et al. Cardiometabolic health outcomes associated with discordant visceral and liver fat phenotypes: insights from the Dallas heart study and UK biobank. *Mayo Clin Proc*. 2022;97(2):225-237.
11. Lv F, Cai X, Li Y, et al. Association between indices of body composition and metabolically unhealthy phenotype in China: a cross-sectional study. *Front Endocrinol*. 2022;13:891327. doi:10.3389/fendo.2022.891327
12. Graffy PM, Pickhardt PJ. Quantification of hepatic and visceral fat by CT and MR imaging: relevance to the obesity epidemic, metabolic syndrome and NAFLD. *Br J Radiol*. 2016;89(1062):20151024. doi:10.1259/bjr.20151024
13. Yamazaki H, Tauchi S, Machann J, et al. Fat distribution patterns and future type 2 diabetes. *Diabetes*. 2022;71(9):1937-1945.
14. Fang H, Berg E, Cheng X, Shen W. How to best assess abdominal obesity. *Curr Opin Clin Nutr Metab Care*. 2018;21(5):360-365.
15. Graffy PM, Sandfort V, Summers RM, Pickhardt PJ. Automated liver fat quantification at nonenhanced abdominal CT for population-based steatosis assessment. *Radiology*. 2019;293(2):334-342.
16. Dietz B, Machann J, Agrawal V, et al. Detection of diabetes from whole-body MRI using deep learning. *JCI Insight*. 2021;6(21):e146999. doi:10.1172/jci.insight.146999
17. Zhou X, Li Y, Zhang X, et al. Independent markers of nonalcoholic fatty liver disease in a gentrifying population-based Chinese cohort. *Diabetes Metab Res Rev*. 2019;35(5):e3156. doi:10.1002/dmrr.3156
18. Zou X, Li Y, Cai X, et al. Decreased glycemic difference between diabetes and nondiabetes in the elderly leads to the reduced diagnostic accuracy of hemoglobin A1c for diabetes screening in an aged Chinese population. *Diabetes Technol Ther*. 2016;18(4):226-232.
19. Pan XF, Wang L, Pan A. Epidemiology and determinants of obesity in China. *Lancet Diabetes Endocrinol*. 2021;9(6):373-392.
20. Kvist H, Chowdhury B, Grangård U, Tylén U, Sjöström L. Total and visceral adipose-tissue volumes derived from measurements with computed tomography in adult men and women: predictive equations. *Am J Clin Nutr*. 1988;48(6):1351-1361.
21. Zhang F, Li Y, Zhao Y, Zhou X, Ji L. Is visceral abdominal fat area a better indicator for hyperglycemic risk? Results from the Pinggu Metabolic Disease Study. *J Diabetes Investig*. 2020;11(4):888-895.
22. Zhang G, Yang Y, Xu S, et al. Autonomous localization and segmentation for body composition quantization on abdominal CT. *Biomed Signal Process Control*. 2022;71:103172. doi:10.1016/j.bspc.2021.103172
23. Graffy PM, Liu J, Pickhardt PJ, Burns JE, Yao J, Summers RM. Deep learning-based muscle segmentation and quantification at abdominal CT: application to a longitudinal adult screening cohort for sarcopenia assessment. *Br J Radiol*. 2019;92(1100):20190327. doi:10.1259/bjr.20190327
24. Cheng X, Zhang Y, Wang C, et al. The optimal anatomic site for a single slice to estimate the total volume of visceral adipose tissue by using the quantitative computed tomography (QCT) in Chinese population. *Eur J Clin Nutr*. 2018;72(11):1567-1575.
25. Okada T, Linguraru MG, Hori M, Summers RM, Tomiyama N, Sato Y. Abdominal multi-organ segmentation from CT images using conditional shape-location and unsupervised intensity priors. *Med Image Anal*. 2015;26(1):1-18.
26. Zou WY, Enchakalody BE, Zhang P, et al. Automated measurements of body composition in abdominal CT scans using artificial intelligence can predict mortality in patients with cirrhosis. *Hepatol Commun*. 2021;5(11):1901-1910.
27. Isensee F, Jaeger PF, Kohl SAA, Petersen J, Maier-Hein KH. nnU-Net: a self-configuring method for deep learning-based biomedical image segmentation. *Nat Methods*. 2021;18(2):203-211.
28. Zhang F. Application of machine learning in CT images and X-rays of COVID-19 pneumonia. *Medicine*. 2021;100(36):e26855. doi:10.1097/MD.0000000000026855
29. Klopfenstein BJ, Kim MS, Krisky CM, Szumowski J, Rooney WD, Purnell JQ. Comparison of 3 T MRI and CT for the measurement of visceral and subcutaneous adipose tissue in humans. *Br J Radiol*. 2012;85(1018):e826-e830.
30. Caussy C, Reeder SB, Sirlin CB, Loomba R. Noninvasive, quantitative assessment of liver fat by MRI-PDFF as an endpoint in NASH trials. *Hepatology*. 2018;68(2):763-772.
31. Guo Z, Blake GM, Li K, et al. Liver fat content measurement with quantitative CT validated against MRI proton density fat fraction: a prospective study of 400 healthy volunteers. *Radiology*. 2020;294(1):89-97.
32. Bydder GM, Chapman RW, Harry D, Bassan L, Sherlock S, Kreel L. Computed tomography attenuation values in fatty liver. *J Comput Tomogr*. 1981;5(1):33-35.
33. Mongraw-Chaffin M, Allison MA, Burke GL, et al. CT-derived body fat distribution and incident cardiovascular disease: the multi-ethnic study of atherosclerosis. *J Clin Endocrinol Metab*. 2017;102(11):4173-4183.
34. Borel AL, Nazare JA, Smith J, et al. Visceral, subcutaneous abdominal adiposity and liver fat content distribution in normal glucose tolerance, impaired fasting glucose and/or impaired glucose tolerance. *Int J Obes (Lond)*. 2005;39(3):495-501.
35. Fabbrini E, Magkos F, Mohammed BS, et al. Intrahepatic fat, not visceral fat, is linked with metabolic complications of obesity. *Proc Natl Acad Sci U S A*. 2009;106(36):15430-15435.
36. Yu F, Fan Y, Sun H, Li T, Dong Y, Pan S. Intermuscular adipose tissue in Type 2 diabetes mellitus: Non-invasive quantitative imaging and clinical implications. *Diabetes Res Clin Pract*. 2022;187:109881. doi:10.1016/j.diabres.2022.109881
37. Granados A, Gebremariam A, Gidding SS, et al. Association of abdominal muscle composition with prediabetes and diabetes: the CARDIA study. *Diabetes Obes Metab*. 2019;21(2):267-275.
38. Lin Z, Feng W, Liu Y, et al. Machine learning to identify metabolic subtypes of obesity: a multi-center study. *Front Endocrinol (Lausanne)*. 2021;12:713592. doi:10.3389/fendo.2021.713592
39. Martin S, Sorokin EP, Thomas EL, et al. Estimating the effect of liver and pancreas volume and fat content on risk of diabetes: a mendelian randomization study. *Diabetes Care*. 2022;45(2):460-468.
40. Lee SS, Park SH, Kim HJ, et al. Non-invasive assessment of hepatic steatosis: prospective comparison of the accuracy of imaging examinations. *J Hepatol*. 2010;52(4):579-585.
41. Grainger AT, Krishnaraj A, Quinones MH, et al. Deep learning-based quantification of abdominal subcutaneous and visceral fat volume on CT images. *Acad Radiol*. 2021;28(11):1481-1487.
42. Schaudinn A, Hudak A, Linder N, et al. Toward a routine assessment of visceral adipose tissue volume from computed tomographic data. *Obesity (Silver Spring)*. 2021;29(2):294-301.

SUPPORTING INFORMATION

Additional supporting information can be found online in the Supporting Information section at the end of this article.

How to cite this article: Zou X, Zhou X, Li Y, et al. Gender-specific data-driven adiposity subtypes using deep-learning-based abdominal CT segmentation. *Obesity (Silver Spring)*. 2023;1-10. doi:10.1002/oby.23741